Synergistic Effects of Radiotherapy With JNK Inhibitor-Incorporated Nanoparticle in an Intracranial Lewis Lung Carcinoma Mouse Models

Chun-Hao Li, Sa-Hoe Lim, Young-Il Jeong, Hyang-Hwa Ryu, and Shin Jung

Abstract— Background: Radiosurgery has been recognized as a reasonable treatment for metastatic brain tumors. Increasing the radiosensitivity and synergistic effects are possible ways to improve the therapeutic efficacy of specific regions of tumors. c-Jun-N-terminal kinase (JNK) signaling regulates H2AX phosphorylation to repair radiation-induced DNA breakage. We previously showed that blocking JNK signaling influenced radiosensitivity *in vitro* and in an *in vivo* mouse tumor model. Drugs can be incorporated into nanoparticles to produce a slow-release effect. This study assessed JNK radiosensitivity following the slow release of the JNK inhibitor SP600125 from a poly (DL-lactide-co-glycolide) (LGEsese) block copolymer in a brain tumor model. Materials and Methods: A LGEsese block copolymer was synthesized to fabricate SP600125-incorporated nanoparticles by nanoprecipitation and dialysis methods. The chemical structure of the LGEsese block copolymer was confirmed by 1H nuclear magnetic resonance (NMR) spectroscopy. The physicochemical and morphological properties were observed by transmission electron microscopy (TEM) imaging and measured with particle size analyzer. The blood-brain barrier (BBB) permeability to the JNK inhibitor was estimated by BBBflammaTM 440-dye-labeled SP600125. The effects of the JNK inhibitor were investigated using SP600125-incorporated nanoparticles and by optical bioluminescence, magnetic resonance imaging (MRI), and a survival assay in a mouse brain tumor model for Lewis lung cancer (LLC)-Fluc cells. DNA damage was estimated by histone γH2AX expression and apoptosis was assessed by the immunohistochemical examination of cleaved caspase 3. Results: The SP600125-incorporated nanoparticles of the LGEsese block copolymer were spherical and released SP600125 continuously for 24h. The use of BBBflammaTM 440-dye-labeled SP600125 demonstrated the ability of SP600125 to cross the BBB. The blockade of JNK signaling with SP600125-incorporated nanoparticles significantly delayed mouse brain tumor growth and prolonged mouse survival after radiotherapy. γH2AX, which mediates DNA repair protein, was reduced and the apoptotic protein cleaved-caspase 3 was increased by the combination of radiation and SP600125-incorporated nanoparticles.

Index Terms— Nanoparticles, JNK, Histon H2AX, radiotherapy, drug delivery.

JNK	c-Jun-N-terminal kinase.
NMR	Nuclear magnetic resonance.
BBB	Blood-brain barrier.
LLC	Lewis lung cancer.
MAPK	Mitogen-activated protein kinase.
LGEsese	Nanoparticles of hyaluronic acid/poly (DL-lactide-co-glycolide).
PLGA	Polyphenol-loaded poly(lactide-co-glycolide).
MePEG	Methoxy poly (ethylene glycol).

Chun-Hao Li is with the Department of Neurosurgery, Yanbian University Affiliated Hospital, Yanji, Jilin 133000, China, and also with the Brain Tumor Research Laboratory, Chonnam National Research Institute of Medical Sciences, Chonnam National University Hwasun Hospital, Hwasun-gun 58128, Jeollanam-do, Republic of Korea (e-mail: lichunhao430@163.com).
Sa-Hoe Lim and Shin Jung are with the Department of Neurosurgery, Chonnam National University Medical School, Hwasun-gun, Jeollanam-do 58128, Republic of Korea, and also with the Brain Tumor Research Laboratory, Chonnam National Research Institute of Medical Sciences, Chonnam National University Hwasun Hospital, Hwasun-gun, Jeollanam-do 58128, Republic of Korea (e-mail: sahoe@jnu.ac.kr; sjung@jnu.ac.kr).
Young-Il Jeong is with the Department of Dental Materials, School of Dentistry, Chosun University, Gwangju 61452, Republic of Korea (e-mail: nanomed@nate.com).
Hyang-Hwa Ryu is with the Department of Biochemistry and Molecular Biology, Jeonbuk National University Medical School, Jeonju-si, Jeollabuk-do 54896, Republic of Korea (e-mail: yy-ryu@hanmail.net).
Digital Object Identifier 10.1109/TNB.2023.3238687

I. INTRODUCTION

METASTATIC brain tumors are cancer that spreads to the brain after initially developing in other parts of the body. With refinements in radiological technology and molecular biology diagnostics, metastatic brain tumors are being increasingly diagnosed and treated early. Radiosurgery has been a standard treatment for brain metastases. However, it has unsatisfactory radiotherapeutic effects that include its large-volume, effects on the brain stem, and the proximity of metastatic brain tumors to important nerves. Increasing radiosensitivity and decreasing the dose of radiation are possible ways to treat tumors to help protect the brain stem and nerves. The development of a nontoxic and efficient

radiosensitizer is necessary. Our previous study showed that blocking c-Jun-N-terminal kinase (JNK) signaling increased radiosensitivity and delayed tumor growth *in vitro* and in an *in vivo* mouse tumor model [1], [2]. With the development of nanobiotechnology, and owing to their unique properties, nanoparticles have become widely explored in cancer therapy. This study explored the therapeutic value of the slow release of an inhibitor of JNK from nanoparticles in an irradiated mouse brain tumor model.

JNK is a subtype of the mitogen-activated protein kinase (MAPK) superfamily [3]. JNK is encoded by three genes (JNK1, 2, and 3), which are spliced into at least 10 isoforms [4], [5]. The JNK protein participates in diverse cellular responses that include the promotion of Bcr-Ab1-induced lymphoma in B-cells [6], the suppression of Ras-induced tumorigenesis in fibroblasts [7], and the phosphorylation of Bcl-2 family proteins or BAD protein to promote or inhibit apoptosis [8], [9]. JNK protein phosphorylates H2AX following ultraviolet irradiation [10]. Histone H2AX is a key factor in the repair of DNA damage after irradiation [11]. The blockade of JNK signaling decreased H2AX phosphorylation and DNA damage and increased radiosensitivity in vestibular schwannoma cells [12], [13]. Our previous data suggested that JNK inhibition also enhanced radiosensitivity and apoptosis following irradiation in a Lewis lung carcinoma subcutaneous tumor model and HVGGSSV-chitoPEGAcHIS-SP600125 selectively targeted irradiated brain tumors and significantly delayed tumor growth [2], [14].

Based on the special physicochemical properties of nano-materials, which have been extensively investigated to improve cancer therapy, nanoparticles of hyaluronic acid/poly (DL-lactide-co-glycolide) (LGEsese) could release their contents in a controlled way and increase anti-invasion efficacy in colorectal cancer cells [14]. Polyphenol-loaded poly(lactide-co-glycolide) (PLGA) nanoparticles also showed controlled drug release and appeared to avoid DNA damage [15]. We previously reported that hyaluronic acid nanoparticles possessed hyaluronidase-specific drug release capability and specifically inhibited cell viability [16]. Furthermore, transferrin-conjugated nanoparticles specifically delivered an anticancer drug to 9L gliosarcoma cells [17]. Therefore, nanoparticles are considered as an appropriate release and delivery system for cancer therapy.

For this study, a di-block copolymer composed of methoxy poly (ethylene glycol) (MePEG) and LGEsese was used to fabricate nanoparticles that slowly released the JNK inhibitor anthra(1,9-cd) pyrazol-6(2H)-one (SP600125). The efficacy of SP600125-incorporated nanoparticles was assessed in the irradiated mouse brain tumor model.

II. MATERIALS AND METHODS

A. Materials

MePEG amine (molecular weight (M.W.): 5,000 g/mol) was purchased from SunBio Co., Ltd. (Seoul, Korea). Poly(DL-lactide-co-glycolide) (PLGA, PLGA-5005, M.W.: 5,000 g/mol) was purchased from Wako Pure Chemical, Co. (Osaka, Japan). Seleno-L-cystine (selenocystine),

N-(3-dimethylaminopropyl)-N´-ethylcarbodiimide hydrochloride (EDAC), and N-hydroxysuccinimide (NHS) were purchased from Sigma-Aldrich, Co. (St. Louis, MO, USA). Dialysis membranes (molecular weight cut-off [MWCO]: 2,000g/mol and 8,000g/mol) were obtained from Spectrum Lab., Inc. (Irvine, CA, USA). All organic solvents, such as dimethylsulfoxide (DMSO), ethyl alcohol, and chloroform, were high-performance liquid chromatography (HPLC) grade.

B. Synthesis of LGEsese Block Copolymer

PLGA (1g) was completely dissolved in 30 ml DMSO and 38.4 mg EDAC and 23 mg NHS were added. This solution was magnetically stirred for 30 h. Selenocystine hydrochloride (33.4 mg) was separately dissolved in a DMSO-water mixture (10 ml DMSO in 4 ml of deionized water) and then added to the PLGA-DMSO solution. These mixtures were magnetically stirred for 48 h. The resulting solution was dialyzed using a dialysis membrane with an MWCO of 8,000 g/mol to remove byproducts for two days with an exchange of water at 3 – 4 h intervals. Lyophilization was used to obtain the PLGA-selenocystine solid (yield > 91%, w/w). The PLGA-selenocystine conjugate (517 mg) was dissolved in 20 ml DMSO with 19.2 mg of EDAC and 11.5 mg of NHS. This solution was magnetically stirred for 24 h and then 600 mg of PEG-amine (1.2 equivalents) was added, followed by magnetic stirring for 30 h. The resulting solution was dialyzed in the aforementioned dialysis membrane to remove byproducts and unreacted MePEG-amine for two days. LGEsese block copolymer solid was obtained by lyophilization (yield 86.2%, w/w).

C. Characterization of LGEsese Block Copolymer

Synthesis of the LGEsese block copolymer was confirmed by 1H nuclear magnetic resonance (NMR) spectroscopy at 500 MHz using a Unity Inova superconducting Fourier transform-NMR spectrometer (Varian Inc., Santa Clara, CA, USA). The morphology of the LGEsese block copolymer nanoparticles was observed using transmission electron microscopy (TEM) with an H-7600 device (Hitachi Instruments Ltd., Tokyo, Japan). An aqueous solution of LGEsese nanoparticles in water was added dropwise on a carbon film-coated copper grid following drying at room temperature. Following this, phosphotungstic acid (0.1%, w/w in deionized water) was dropped onto the copper grid to negatively stain the nanoparticles. Nanoparticle observation was conducted at 80 kV. The nanoparticle size was measured with the Nano-ZS apparatus (Malvern, Worcestershire, UK). Nanoparticles in deionized water were used to measure the particle size at room temperature.

D. Preparation of SP600125-Incorporated LGEsese Nanoparticles

SP600125-incorporated nanoparticles were fabricated. LGEsese block copolymer (100 mg) was dissolved in 10 ml of acetone and 6 or 10 mg of SP600125 was added to the solution. The solution was slowly dispensed in 30 ml

of deionized water with magnetic stirring. The solvent was removed by rotary evaporation using an EYELA N-1100 apparatus (Tokyo Rikakikai Co. Ltd., Tokyo, Japan). To remove the remaining solvent and un-loaded drug, the solution was further dialyzed against distilled water for 12 h with the exchange of water at 1-h intervals. Finally, the dialyzed solution was used to analysis, drug release study, or lyophilization for 2 days. Empty nanoparticles were similarly fabricated in the absence of the drug. The drug contents were estimated as follows. Nanoparticles (5 mg) were dissolved in 10 ml of DMSO and this solution was used to measure the SP600125 contents in the nanoparticles. SP600125 in DMSO was measured using an ultraviolet-visible (UV-VIS) spectrophotometer (UV-1601; Shimadzu Co., Tokyo, Japan) at 403 nm. Empty nanoparticles were used for blank test. The drug contents were calculated as (drug weight/nanoparticle weight) $\times$ 100.

E. SP600125 Release Assay

Lyophilized SP600125-incorporated nanoparticles were reconstituted in 5 ml of deionized water and added to a dialysis membrane with an MWCO of 2,000 g/mol. The sealed membrane was added to a bottle containing 95 ml of phosphate-buffered saline (PBS, pH 7.4, 0.01M). At specified times, PBS was removed and used to measure the concentration of the released SP600125. An equivalent volume of fresh PBS was added to avoid drug saturation. The released SP600125 was measured at 403 nm with the aforementioned UV-VIS spectrophotometer. Empty nanoparticles were also used in the drug release test and PBS was used as the blank.

F. Cell Cultures and Treatment Conditions

Murine Lewis lung cancer (LLC) cells were obtained from the American Type Culture Collection (Manassas, VA, USA). LLC cells were transfected with a lentiviral vector containing a firefly luciferase (Fluc) gene (a gift from Professor Min, Hwasun Chonnam National University Hospital, Korea). The cells were cultured in Dulbecco's modified Eagle's medium (DMEM; Gibco BRI) supplemented with 10% fetal bovine serum (FBS) (GibcoBRL, Gaithersburg, MD, USA) in a 37°C air incubator.

G. Toxicity of the Nanoparticles

The toxicity of empty nanoparticles and SP600125-incorporated nanoparticles was monitored by a standard 3-(4,5-dimethylthiazol-2-yl)-2,5-diphenyl tetrazolium bromide (MTT) assay. LLC-Fluc cells (103 cells/well) were cultured in 96-well plates in 100 μl of medium under standard conditions. At 48 h, 10 μl of MTT reagent (5 mg/ml PBS) was added to each well. After 2 h, the medium was removed and added to 200 μl of DMSO to solubilize MTT formazan. The optical density was measured at 570 nm.

H. Bioluminescence Imaging

Imaging was performed using a NightOWL animal imaging measurement system (Bertholdtechnologies, Bad Wildbad,

Germany) equipped with a cooled charge-coupled device camera to acquire bioluminescent images of the mouse brain tumor. The photons emitted from the luciferase-expressing tumor cells were collected for 2 min. The pseudocolor images of the photons were measured by the IndiGo program (Berthold Technologies). The regions of interest were automatically chosen based on the signal.

I. Blood-Brain Barrier (BBB) Permeability Assay

Seven-week-old male BALB/c – nu/nu mice were obtained from Orientbio (Seongnam, Korea). Fluorescence imaging was performed using the NightOWL imaging system (Berthold Technologies) equipped with a filter set (excitation at 475 nm and emission at 520 nm). BBBflammaTM 440 dye (molecular weight 500.61 g/mol) and BBBflammaTM 440-labeled SP600125 (molecular weight 803.94 g/mol) were kindly obtained from BioActs, Co. (Incheon, Korea). The drugs were intravenously and intraperitoneally injected (1 mg/kg) into mice. The mice were euthanized and the brain tissue was removed and scanned with an optical imager 24 h after drug injection. Image analysis was performed using the IndiGo program.

J. Animal Studies

Seven-week-old C57BL/6 female mice were obtained from Orientbio. LLC-Fluc cells (2 $\times$ 105) were diluted in 3 μl of PBS and inoculated (1 μl/min) into the right side of the brains of mice at an injection depth of 3 mm. At the end of the injection, the syringe was maintained for three minutes to ensure that the cells did not overflow. Bone wax was used to close the skull hole. Irradiation and intraperitoneal injections of SP600125-incorporated nanoparticles (70 mg per mouse in a single application) were carried out 5 – 7 days after the cancer cell injections. The whole mouse brain was irradiated with a fractionated schedule (3 $\times$ 6.1 Gy, total 13 Gy) using a 6-MV X-ray linear accelerator (CLINAC 21EX; Varian, Palo Alto, CA, USA). The effects of the JNK inhibitor were investigated by optical bioluminescence, magnetic resonance imaging (MRI), and hematoxylin and eosin (H&E) staining 8 – 10 days after the start of radiotherapy. The survival of the mice was monitored.

K. Immunohistochemistry

Immunohistochemical analysis was performed as previously described (16, 17). The mice were euthanized and brain tissue was removed 24 h after radiotherapy (6.1 Gy). The mouse brain tissue specimens were dewaxed in xylene and heat-mediated antigen retrieval in the target solution (pH 9.0, Dako, Carpentaria, CA, USA) was performed for 12 min. The endogenous peroxidase activity was blocked in 3% H2O2 in PBS for 30 min. Non-specific binding was blocked using 5% horse serum (Sigma-Aldrich). Primary antibodies anti-cleaved caspase-3 (Cell Signaling Technology, Danvers, MA, USA) and anti-phosphorylated Ser139 histone H2AX (Cell Signaling Technology) were applied at 4 °C overnight. A secondary antibody (Dako) was added for 2 h followed by
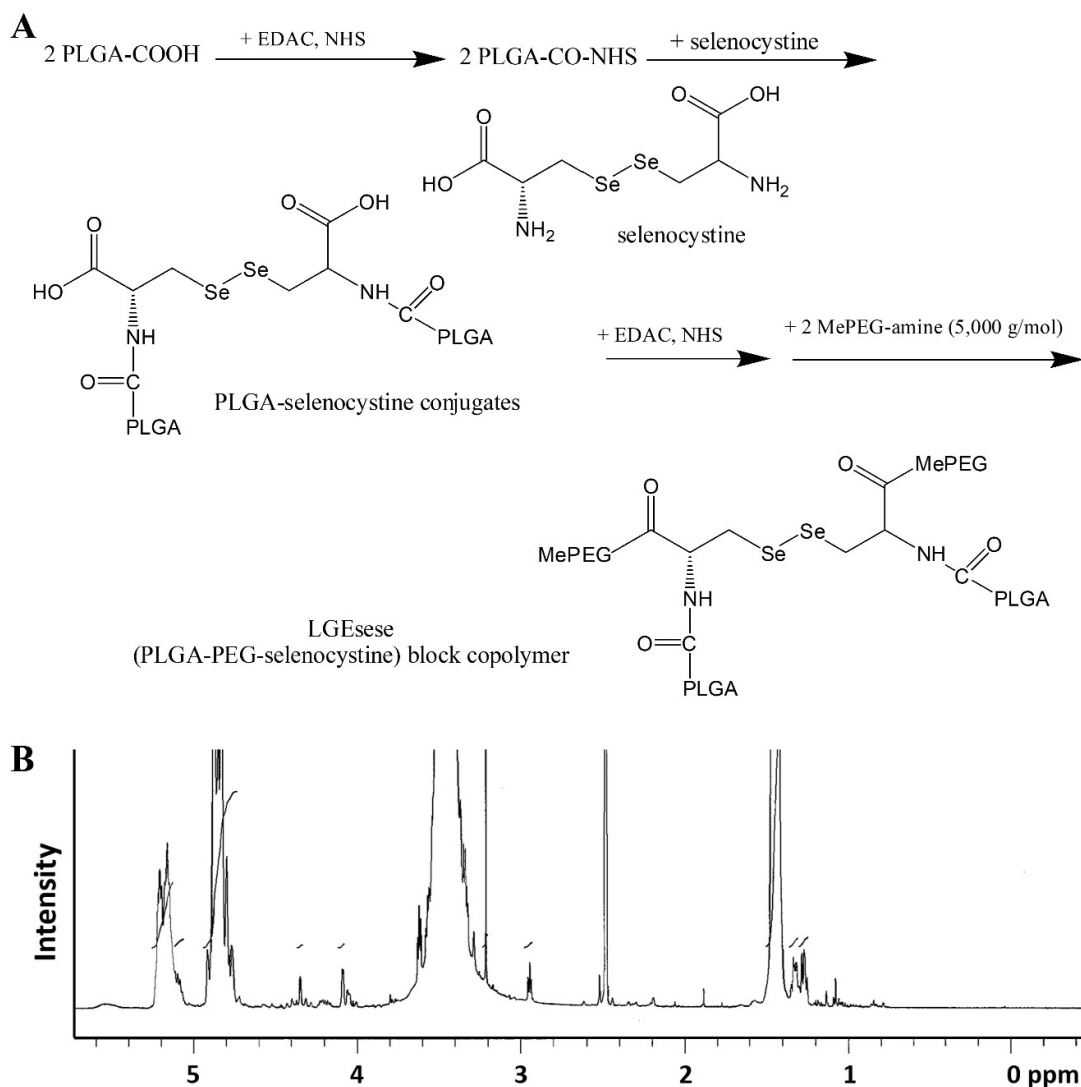
Fig. 1. A: synthesis scheme and B: ^{1}H NMR spectra of LGE block copolymer.

3,3'-diaminobenzidine (Dako). The nuclei were stained with Harris hematoxylin (ScyTek, Logan, UT, USA).

L. Statistical Analyses

The data are shown as the mean $\pm$ SD. The comparisons between the two groups were analyzed using the Student's t-test. Log-rank analysis was performed to establish the statistical significance of the Kaplan–Meier survival curve analyses. A probability value of < 0.05 was considered significant.

III. RESULTS

A. Characterization of LGEsese Block Copolymer and SP600125-Incorporated Nanoparticles

Figure 1A shows the synthesis scheme of the LGEsese block copolymer and 1H nuclear magnetic resonance (NMR) spectra. As shown in Figure 1B, the carboxylic acid end of PLGA was activated by carbodiimide chemistry and conjugated with the amine group of selenocystine. The specific peak of selenocystine was confirmed at 1.9 ppm and the

methyl group of the lactide segment in PLGA was confirmed at 1.4-1.5 ppm. The carboxylic acid groups of the PLGA-selenocystine conjugates were activated again with N-(3-dimethylaminopropyl)-N′-ethylcarbodiimide hydrochloride (EDAC) and N-hydroxysuccinimide (NHS). Following this, the NHS-activated PLGA-selenocystine conjugates were conjugated with the amine group of MePEG. Ethylene protons of PEG were confirmed at 3.3-3.6 ppm. The final yield of LGEsese block copolymer was 86.2%, w/w.

SP600125-incorporated nanoparticles of the LGEsese block copolymer were fabricated by nanoprecipitation and dialysis. The physicochemical characteristics of the nanoparticles are summarized in Table I. Since SP600125 is a hydrophobic agent, it can be associated with PLGA segment of block copolymer and then formed hydrophobic core in the nanoparticles while PEG segment formed hydrated outer-shell. Then, experimental drug contents in the nanoparticles were 4.1 and 6.2% (w/w). The experimental drug contents were lower than the theoretical values. These results were due to that unloaded drug during nanoprecipitation and loaded drug in the

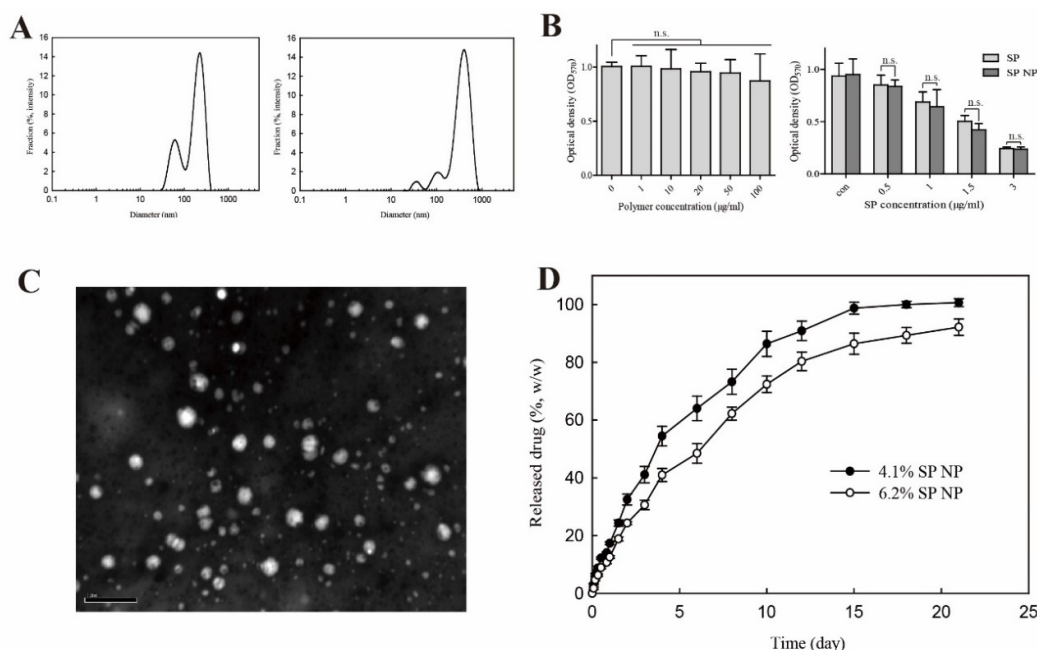| Polymer/drug ratio (mg/mg)	Drug contents		Particle size (nm)
	Theoretical	Experimental	
100/6	5.7	4.1	285
100/10	9.1	6.2	386

Fig. 2. Characterization of LGEsese block copolymer and SP600125-incorporated nanoparticles. A: Particle size of SP600125-incorporated nanoparticles for 4.1 % and 6.2 %. B: Toxicity assay of empty nanoparticles and SP600125-incorporated nanoparticles. C: TEM photograph of SP600125-incorporated nanoparticles (6.2 %). D: The SP600125 release rate from LGEsese nanoparticles. Bars indicate ± SD; columns, mean; SP, SP600125; SP NP, SP600125-incorporated nanoparticles; n.s., not significant.

nanoparticles muse be removed from the dialysis tube and then these procedures induced lower values in experimental drug contents that those in theoretical value. Even though SP600125 is a hydrophobic agent, it can be also removed in the procedure of organic solvent removal from the dialysis membrane.

Higher drug content increased the particle size. The size of the nanoparticles with 4.1% and 6.2% (w/w) SP600125 was 285 and 386 nm, respectively (Fig. 2A). TEM examination revealed the spherical shape of the nanoparticles (Fig. 2C), which was <300 nm in diameter. As shown in Figure 2D, Sp600125 was released from the nanoparticles over a 21-day interval. The release occurred as an initial burst for the first four days, with continuous release thereafter in different rate depending upon the drug loading. Nanoparticles loaded with 4.1% (w/w) SP600125 released almost all the drug by 15 days, whereas the nanoparticles containing 6.2% (w/w) SP600125 showed a delayed release rate over 21 days. The SP600125-incorporated nanoparticles with 6.2% (w/w) SP600125 were selected for the next experiments.

B. Toxicity Assay

In the empty nanoparticles, cell growth was not affected by increasing nanoparticle concentrations up to 100 μg/ml (Fig. 2B). The toxicity of SP600125 was compared in isolation and when incorporated into nanoparticles. Cell growth was dose-dependently inhibited in the presence of isolated SP600125, with growth nearly halted in culture medium containing 3 μg/ml SP600125 (Fig. 2B). After SP600125 was incorporated into nanoparticles, cell growth was inhibited further with increasing concentrations of SP600125. SP600125 toxicity was not enhanced by encapsulation into the core of the nanoparticles.

C. BBB Passage of SP600125

To estimate the BBB permeability to the JNK inhibitor SP600125, BBBflammaTM 440 dye alone and BBBflammaTM 440-labeled SP600125 were intravenously and intraperitoneally injected into mice. The fluorescence concentration increased in the intravenously and intraperitoneally
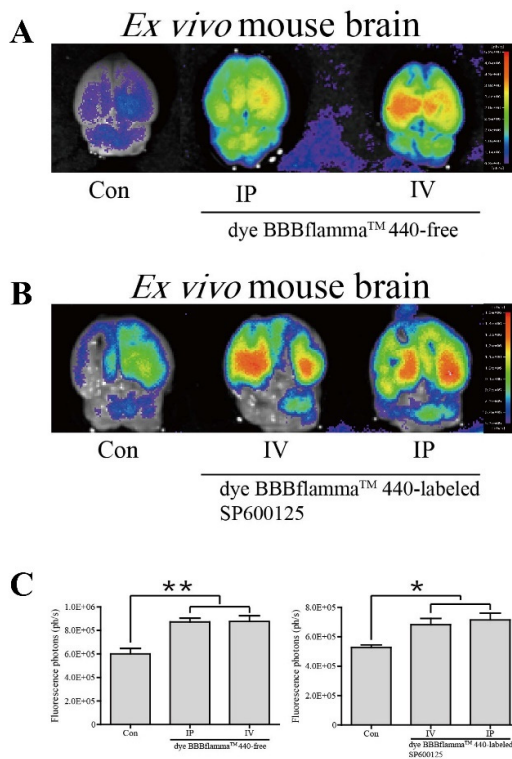
Fig. 3.   IVIS optical imaging study for (A) dye BBBflammaTM 440-free and (B) dye BBBflammaTM 440-labeled SP600125 injection. Mice brains were sacrificed and scanned at 24h after injection of dye. (C): The fluorescent dyes exhibited significantly higher in the drug-injected mice brain. Notes: *P<0.05; ***P<0.001.

injected groups compared to the control group (Fig. 3). The results indicated that both the BBBflammaTM 440 dye and SP600125 could cross the BBB.

D. Combination of SP600125-Incorporated Nanoparticles With Fractionated Irradiation Delays Lewis Lung Cancer Tumor Growth in the Mouse Brain Tumor Model

SP600125 effects were confirmed *in vitro* and in the subcutaneous mouse tumor model. The effects of SP600125 incorporated into nanoparticles were further investigated in the mouse brain tumor model. We established the bioluminescent Lewis lung cancer (LLC)-Fluc cell line for this *in vivo* study. The LLC-Fluc cells emitted photons when D-luciferin was added (Fig. 4A). As shown in Figures 4B and C, the bioluminescence photons were not significantly changed in the treatment with SP600125-incorporated nanoparticles compared to the vehicle group. However, the combination of SP600125-incorporated nanoparticles with fractionated irradiation showed significantly decreased bioluminescent imaging photons compared to the radiation group. Furthermore, the combination therapy obviously delayed the tumor growth as assessed by magnetic resonance imaging (MRI) and hematoxylin and eosin (H&E) staining (Fig. 4D). The immunohistochemistry results showed that the level of γH2AX was decreased in the combined treatment compared to radiation

alone. The expression of cleaved caspase-3 was increased in the combined SP600125 and radiation treatment group compared to the other groups (Fig. 5A). The analysis of mouse survival showed that the median survival was 18.8 days for the control group, 19.4 days for the SP600125-nanoparticles group, 31.1 days for the radiation group, and 36 days for the combined radiation and SP600125-nanoparticle group. Treatment with only SP600125-nanoparticles did not noticeably affect the survival of mice, whereas radiation and SP600125-nanoparticles significantly prolonged survival (Fig. 5B).

IV. DISCUSSION

Brain metastases are malignant and the most common tumor in the brain. Twenty to forty percent of cancer patients are diagnosed with metastatic brain tumors, with about 39% originating from lung cancer [18], [19]. The general therapeutic modalities of brain metastases include surgery, radiosurgery, and chemotherapy. Gamma knife stereotactic radiosurgery is the gold standard treatment for metastatic brain tumors [20]. However, the large size and specific region of the tumor can lead to the use of an inadequate radiation dose because the brain stem and important nerves are vulnerable to radiation. Therefore, the research and development of new radiosensitizers are essential. Our previous study indicated that the blockade of JNK activity increased radiosensitivity *in vitro* and in an *in vivo* mouse tumor model [1]. However, the requirement for daily injection of the drug was intractable for human therapeutic use. Presently, the use of SP600125-incorporated nanoparticles had made the therapy more relevant for human use.

Radiation induces a wide variety of DNA lesions, including single-strand breaks (SSBs) and double-strand breaks (DSBs). DSBs are a major source of radiotoxicity damage that is responsible for cell death [21], [22], [23]. In addition, DSBs may lead to human disorders including cancer by chromosomal aberrations [24]. The histone H2AX comprises approximately 2 – 25% of the histone H2A pool in mammalian cells and nucleosomes, and DSBs induce the histone H2AX phosphorylation of serine 139 [25]. The core histones in the nucleosome are H2A, H2B, H3, and H4 [26]. The H2A family comprises histone proteins H2A1, H2A2, H2AZ, and H2AX [27]. H2AX plays an important role in the DNA repair of DSBs, particularly after irradiation [28]. H2AX phosphorylation occurs within seconds after DSBs, which are induced by radiation for 15-30 min [29]. H2AX is phosphorylated by ataxia telangiectasia mutated protein (ATM), ATM and Rad 3-related protein (ATR), and DNA-dependent protein kinase (DNA-PK) [30], [31]. In addition, JNK is involved in H2AX phosphorylation [10]. γH2AX recruits DNA repair-enabling proteins, such as Nbs1, 53BP1, Rad50, Rad51, and Brac1, to repair DNA damage [32]. JNK is a member of the MAPK superfamily. It consists of 10 forms, with three slicing variant isoforms (JNK1, JNK2, JNK3, and JNK4) [5]. JNK1 and JNK2 are ubiquitously expressed in all cell and tissue types, while JNK3 is specifically found in neuronal and heart tissues, all of which have two different splicing forms (p46 and P54) [33], [34]. The small-molecule inhibitor
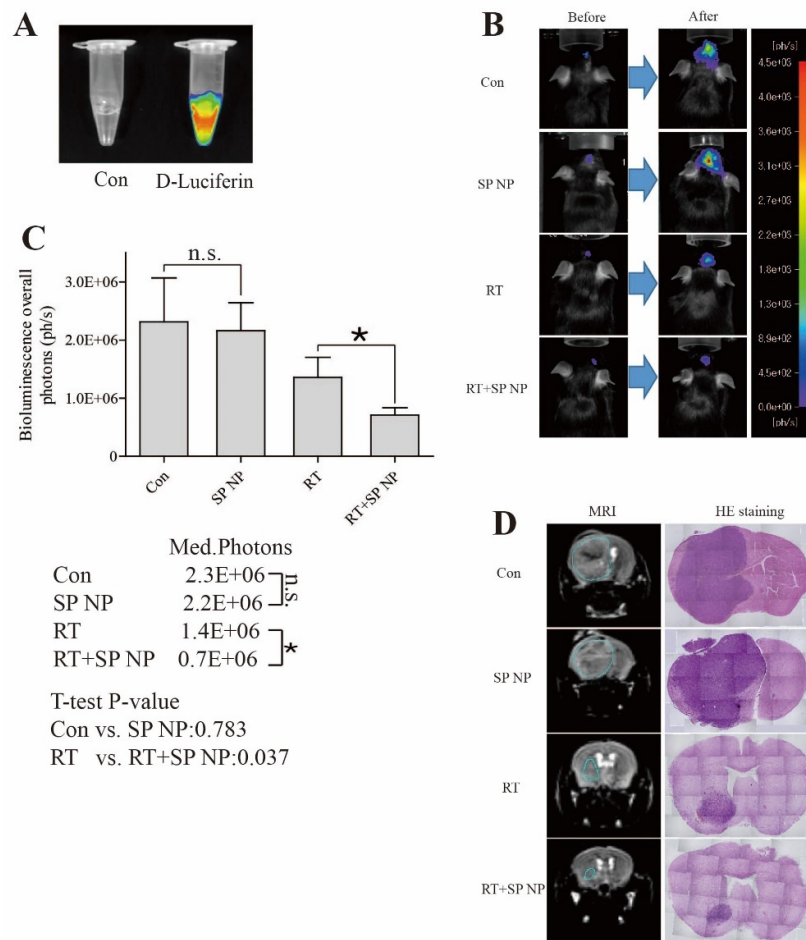
Fig. 4. Combination of SP600125-incorporated nanoparticles with fractionated irradiation delayed LLC tumor growth in mouse brain tumor model. A: photons emitted from LLC-Fluc cell line when D-luciferin was added; B: The LLC-Fluc bearing mice brain were continuously observed by tumor bioluminescence. C: Quantitative analysis of bioluminescence in brain tumor model as shown B. D: The MRI and HE staining imaging results of brain model. The mice were irradiated with fractionated schedule (3×6.1 Gy). Bars indicate $\pm$ SD; columns, mean; SP NP, SP600125-incorporated nanoparticles; RT, radiation; n.s., not significant; *p < 0.05.

SP600125 is a selective inhibitor of JNK, in which ATP competitively and reversibly inhibits the phosphorylation of JNK1, JNK2, and JNK3 [35], [36]. Our previous study indicated that JNK and γH2AX were increased in radiated LLC cells as a means of repairing DNA damage and that SP600125 blocked JNK signaling and significantly decreased γH2AX expression [1]. Another JNK inhibitor, PGL5001, has undergone a phase Ï clinical trial of inflammatory endometriosis (clinicaltrials.gov ID: NCT01630252). It is hoped that the present results will prompt a clinical trial for SP600125.

Reactive oxygen species (ROS) are induced by radiation in the early and late ($2 - 8$ days) stages and disrupt biopolymers [37], [38]. ROS generally includes free radicals, such as hydroxyl radicals ($\bullet$OH) and superoxide anions ($O2\bullet-$), and non-radical molecules like singlet oxygen ($^1O_2$) and H_2O_2, all of which are able to damage various molecular targets including DNA, proteins, and lipids [39], [40]. ROS are especially harmful to cells at high concentrations. The enhanced production of ROS can pose a threat by causing the oxidation of proteins, the peroxidation of lipids, damage to nucleic acids,

and the inhibition of enzymes, which ultimately leads to cell death [41], [42]. ROS generation is enhanced by radiation and induces cell apoptosis via the mitochondrial pathway with increased caspase-3 activity [12], [13], [43]. Similarly, our previous data indicated that the blockade of JNK signaling increased apoptosis in radiated LLC cells.

With the development of nanobiotechnology, nanoparticles have been investigated as drug carriers. The potentials of nanoparticles include their use in various drug formulations, controlled drug release, drug targeting against specific body sites. Due to the small particle size and active/passive targeting potential, nanoparticles have been extensively investigated as drug carriers [49], [50]. The discovery of biomolecular markers that are specifically expressed in cancer has improved the understanding of cancer cells and targeted cancer therapy [51]. Dual-targeting ligands (angiopep-2 and activatable cell-penetrating peptide (ACP)) have been functionalized onto nanoparticles for glioma-targeting treatment [52]. Dual peptide-modified liposomes were designed by attaching two receptor-specific peptides, specifically Angiopep-2 and tLyP-1
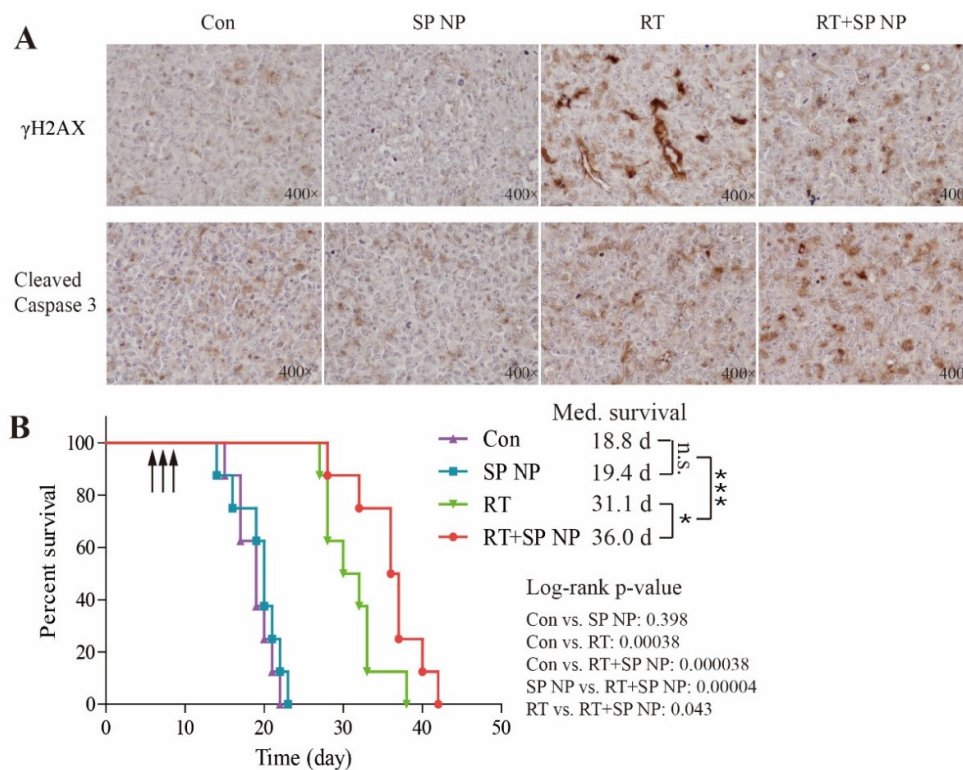
Fig. 5. JNK inhibition increased DNA damage and apoptosis as well as improved survival in irradiated LLC mouse brain model. A: Expression of γH2AX and Cleaved-Caspase 3. The mice sacrificed and removed brain tissue at 24h after radiotherapy (6.1 Gy). B: Kaplan-Meier survival curves for mouse brain tumor model. The mice were irradiated with fractionated schedule (3×6.1 Gy) on consecutive days ($n = 8$ in each group). The arrows indicate time of radiation. SP NP, SP600125-incorporated nanoparticles; RT, radiation; Med. survival, median survival; n.s., not significant by Log-rank test; *$p < 0.05$; ***$p < 0.0001$.

for brain tumor targeting and penetration, and when used with docetaxel for killing of glioma tumor cells [53]. Nanoparticles have also been used in the development of radioprotection drugs [54]. Clinical approaches utilizing nanotechnology have demonstrated that drug delivery systems can increase efficacy, simultaneously reduce side effects, and improve targeted delivery and active cellular uptake of bioactive molecules [55]. Our previous data suggested that HVGGSSV-chitoPEGAcHIS-SP600125 selectively targeted irradiated brain tumors and significantly delayed tumor growth [2].

Nanoparticles designed in the present study featured the slow release of the incorporated material. A LGEsese block copolymer was synthesized to fabricate SP600125-incorporated nanoparticles by nanoprecipitation and dialysis methods. The final yield of LGEsese block copolymer was 86.2%, w/w. NMR spectroscopy revealed that the LGEsese block copolymer was successfully synthesized. SP600125-incorporated nanoparticles of the LGEsese block copolymer were fabricated by nanoprecipitation and dialysis. The experimental drug contents were lower than the theoretical values because unloaded drug during nanoprecipitation and loaded drug in the nanoparticles muse be removed from the dialysis tube. For the drug contents of nanoparticle, the percent difference was -31.8% based on the theoretical value. This is somewhat improved result considering that it was -38.5% in our previous study. We investigated the radiosensitivity effects of SP600125 incorporated into the nanoparticles in an established mouse brain tumor model.

The delivery of drugs to brain tissue or brain tumors necessitates passage through the BBB. The BBB is a diffusion barrier in the brain that impedes the influx of most compounds from the blood. Examining drug permeability is challenging. The structural components that modulate permeability were assessed in an *in vitro* model to detect BBB permeability [44]. In addition, a primary endothelial cell BBB model was used [45], [46]. However, the direct detection of BBB permeability is more difficult *in vivo*. Much of the present research is focused on the effects of drugs in BBB permeability, such as Evan's blue dye that was used in examining BBB permeability [47]. Evan's blue dye crosses the BBB, but it cannot detect BBB permeability. Xiong at al. reported that cy5.5 dye (molecular weight 1128.4 g/mol) and a cy5.5-labeled peptide crossed the BBB [48]. However, cy5.5 and/or cy5.5-labeled macromolecules seem to be difficult to cross BBB since the molecular weight of cy5.5 is higher than conventional fluorescent dye such as fluorescein isocyanate (FITC) or Evan's blue dye.

In this research, we synthesized the small molecular dye BBBflammaTM 440 to estimate the BBB permeability to JNK inhibitor SP600125. BBBflammaTM 440-labeled SP600125 (molecular weight 803.94 g/mol)were intravenously and intraperitoneally injected into mice. The fluorescence

concentration significantly increased in the drug-injection groups compared to the control group. This result suggest that SP600125 was able to cross the BBB and thus, might be used for the treatment of brain tumors.

We showed that SP600125-incorporated LGEsese nanoparticles can advance intratumoral biodistribution of nanoradiosensitizer and enhance tumor bioavailability, resulting in improved brain tumor growth delay. The median survival analysys of mice showed that the survival period of the combined radiation and SP600125-nanoparticles group was increased by 16% compared to the radiation only group [p<0.05]. These results indicated that the blockade of JNK signaling with SP600125 significantly can delay mouse brain tumor growth and prolonged survival in radiotherapy.

V. CONCLUSION

The SP600125-incorporated nanoparticles showed a delayed release rate over 21 days. SP600125 inhibited JNK activity and suppressed DNA repair of radiation as a radiosensitizer, which delayed irradiated brain tumor growth. These results suggest that SP600125-loaded nanoparticles could be a therapeutic candidate in combination with radiotherapy for the treatment of metastatic brain.

VI. PATENTS

AUTHOR CONTRIBUTIONS

Conception and design: Chun-Hao Li, Sa-Hoe Lim, and Shin Jung. Analysis and interpretation of data: Chun-Hao Li, Sa-Hoe Lim, Young-Il Jeong, Hyang-Hwa Ryu, and Shin Jung. Administrative/technical/material support: Chun-Hao Li, Sa-Hoe Lim, Young-Il Jeong, and Hyang-Hwa Ryu. Study supervision: Shin Jung.

CONFLICTS OF INTEREST

The authors declare no conflicts of interest.

REFERENCES

[1] C.-H. Li, S.-H. Lim, H.-H. Ryu, K.-S. Moon, T.-Y. Jung, and S. Jung, "Enhancement of radiosensitivity by inhibition of c-Jun N-terminal kinase activity in a Lewis lung carcinoma-bearing subcutaneous tumor mouse model," *Oncol. Rep.*, vol. 36, no. 6, pp. 3397–3404, Nov. 2016.

[2] S. H. Lim, "Enhancing radiotherapeutic effect with nanoparticle-mediated radiosensitizer delivery guided by focused gamma rays in Lewis lung carcinoma-bearing mouse brain tumor models," *Int. J. Nanomed.*, vol. 14, pp. 8861–8874, 2019.

[3] M. Hibi, "Identification of an oncoprotein- and UV-responsive protein kinase that binds and potentiates the c-Jun activation domain," *Genes Develop.*, vol. 7, no. 11, pp. 2135–2148, 1993.

[4] S. Gupta, "Selective interaction of JNK protein kinase isoforms with transcription factors," *EMBO J.*, vol. 15, no. 11, pp. 2760–2770, 1996.

[5] R. J. Davis, "Signal transduction by the JNK group of MAP kinases," *Cell*, vol. 103, no. 2, pp. 239–252, 2000.

[6] P. Hess, "Survival signaling mediated by c-Jun NH$_2$-terminal kinase in transformed B lymphoblasts," *Nature Genet.*, vol. 32, no. 1, pp. 201–205, 2002.

[7] N. J. Kennedy, "Suppression of Ras-stimulated transformation by the JNK signal transduction pathway," *Genes Develop.*, vol. 17, no. 5, pp. 629–637, 2003.

[8] K. Maundrell et al., "Bcl-2 undergoes phosphorylation by c-Jun N-terminal kinase/stress-activated protein kinases in the presence of the constitutively active GTP-binding protein Rac1," *J. Biol. Chem.*, vol. 272, no. 40, pp. 25238–25242, 1997.

[9] C. Yu et al., "JNK suppresses apoptosis via phosphorylation of the proapoptotic Bcl-2 family protein BAD," *Mol. Cell*, vol. 13, no. 3, pp. 329–340, 2004.

[10] C. Lu et al., "Cell apoptosis: Requirement of H2AX in DNA ladder formation, but not for the activation of caspase-3," *Mol. Cell*, vol. 23, no. 1, pp. 121–132, 2006.

[11] J. Kobayashi, "Molecular mechanism of the recruitment of NBS1/hMRE11/hRAD50 complex to DNA double-strand breaks: NBS1 binds to γ-H2AX through FHA/BRCT domain," *J. Radiat. Res.*, vol. 45, no. 4, pp. 473–478, 2004.

[12] W. Y. Yue, "Contribution of persistent c-Jun N-terminal kinase activity to the survival of human vestibular schwannoma cells by suppression of accumulation of mitochondrial superoxides," *Neuro Oncol.*, vol. 13, no. 9, pp. 961–973, 2011.

[13] W. Y. Yue, "Inhibition of c-Jun N-terminal kinase activity enhances vestibular schwannoma cell sensitivity to gamma irradiation," *Neuro-surgery*, vol. 73, no. 3, pp. 506–516, 2013.

[14] Y. I. Jeong et al., "Self-assembled nanoparticles of hyaluronic acid/poly (DL-lactide-co-glycolide) block copolymer," *Colloids Surf. B, Biointerfaces*, vol. 90, pp. 28–35, Feb. 2012.

[15] A. K. Srivastava, "Synthesis of PLGA nanoparticles of tea polyphenols and their strong in vivo protective effect against chemically induced DNA damage," *Int. J. Nanomed.*, vol. 8, pp. 1451–1462, Jan. 2013.

[16] Y. I. Jeong et al., "Cisplatin-incorporated hyaluronic acid nanoparticles based on ion-complex formation," *J. Pharm. Sci.*, vol. 97, no. 3, pp. 1268–1276, 2008.

[17] Y. I. Jeong, "Delivery of transferrin-conjugated polysaccharide nanoparticles in 9L gliosacoma cells," *J. Nanosci. Nanotechnol.*, vol. 15, no. 1, pp. 125–129, 2015.

[18] N. U. Lin, J. R. Bellon, and E. P. Winer, "CNS metastasis in breast cancer," *J. Clin. Oncol.*, vol. 22, no. 17, pp. 3608–3617, 2004.

[19] I. T. Gavrilovic and J. B. Posner, "Brain metastases: Epidemiology and pathophysiology," *J. Neuro-Oncol.*, vol. 75, no. 1, pp. 5–14, Oct. 2005.

[20] M. A. Hatiboglu, "Treatment of high numbers of brain metastases with Gamma Knife radiosurgery: A review," *Acta Neurochir.*, vol. 158, no. 4, pp. 625–634, 2016.

[21] J. Vignard and G. B. M. Salles, "Ionizing-radiation induced DNA double-strand breaks: A direct and indirect lighting up," *Radiother. Oncol.*, vol. 108, no. 3, pp. 362–369, 2013.

[22] J. Cadet and T. J. L. D. Ravanat, "Oxidatively generated damage to the guanine moiety of DNA: Mechanistic aspects and formation in cells," *Accounts Chem. Res.*, vol. 41, no. 8, pp. 1075–1083, 2008.

[23] A. Kumar, "Sesamol ameliorates radiation induced DNA damage in hematopoietic system of whole body γ-irradiated mice," *Environ. Mol. Mutagenesis*, vol. 59, no. 1, pp. 79–90, 2018.

[24] S. P. Jackson and J. Bartek, "The DNA-damage response in human biology and disease," *Nature*, vol. 461, no. 7267, pp. 1071–1078, 2009.

[25] E. P. Rogakou, D. R. Pilch, A. H. Orr, V. S. Ivanova, and W. M. Bonner, "DNA double-stranded breaks induce histone H2AX phosphorylation on serine 139," *J. Biol. Chem.*, vol. 273, no. 10, pp. 5858–5868, 1998.

[26] E. R. Foster and J. A. Downs, "Histone H2A phosphorylation in DNA double-strand break repair," *FEBS J.*, vol. 272, no. 13, pp. 3231–3240, 2005.

[27] J. Ausio and D. W. Abbott, "The many tales of a tail: Carboxyl-terminal tail heterogeneity specializes histone H2A variants for defined chromatin function," *Biochemistry*, vol. 41, no. 19, pp. 5945–5949, 2002.

[28] J. A. Downs, N. F. Lowndes, and S. P. Jackson, "A role for *Saccharomyces cerevisiae* histone H2A in DNA repair," *Nature*, vol. 408, no. 6815, pp. 1001–1004, 2000.

[29] M. Lobrich et al., "γH2AX foci analysis for monitoring DNA double-strand break repair: Strengths, limitations and optimization," *Cell Cycle*, vol. 9, no. 4, pp. 662–669, 2010.

[30] H. Wang, M. Wang, H. Wang, W. Böcker, and G. Iliakis, "Complex H2AX phosphorylation patterns by multiple kinases including ATM and DNA-PK in human cells exposed to ionizing radiation and treated with kinase inhibitors," *J. Cellular Physiol.*, vol. 202, no. 2, pp. 492–502, Feb. 2005.

[31] S. Burma, B. P. Chen, M. Murphy, A. Kurimasa, and D. J. Chen, "ATM phosphorylates histone H2AX in response to DNA double-strand breaks," *J. Biol. Chem.*, vol. 276, no. 45, pp. 42462–42467, 2001.

[32] S. E. Polo and S. P. Jackson, "Dynamics of DNA damage response proteins at DNA breaks: A focus on protein modifications," *Genes Develop.*, vol. 25, no. 5, pp. 409–433, 2011.

[33] A. Lin, "Activation of the JNK signaling pathway: Breaking the brake on apoptosis," *BioEssays*, vol. 25, no. 1, pp. 17–24, Jan. 2003.

[34] A. M. Bode and Z. Dong, "The functional contrariety of JNK," *Mol. Carcinog.*, vol. 46, no. 8, pp. 591–598, 2007.

[35] B. L. Bennett, "SP600125, an anthrapyrazolone inhibitor of Jun N-terminal kinase," *Proc. Nat. Acad. Sci. USA*, vol. 98, no. 24, pp. 13681–13686, 2001.

[36] Q. H. Guan, D. S. Pei, Q. G. Zhang, Z. B. Hao, T. L. Xu, and G. Y. Zhang, "The neuroprotective action of SP600125, a new inhibitor of JNK, on transient brain ischemia/reperfusion-induced neuronal death in rat hippocampal CA1 via nuclear and non-nuclear pathways," *Brain Res.*, vol. 1035, no. 1, pp. 51–59, 2005.

[37] Z. Gao, E. H. Sarsour, A. L. Kalen, L. Li, M. G. Kumar, and P. C. Goswami, "Late ROS accumulation and radiosensitity in SOD1-overexpressing human glioma cells," *Free Radical Biol. Med.*, vol. 45, no. 11, pp. 1501–1509, 2008.

[38] O. Loseva, E. Shubbar, S. Haghdoost, B. Evers, T. Helleday, and M. Harms-Ringdahl, "Chronic low dose rate ionizing radiation exposure induces premature senescence in human fibroblasts that correlates with up regulation of proteins involved in protection against oxidative stress," *Proteomes*, vol. 2, no. 3, pp. 341–362, Jul. 2014.

[39] N. R. Jena, "DNA damage by reactive species: Mechanisms, mutation and repair," *J. Biosci.*, vol. 37, no. 3, pp. 503–517, 2012.

[40] P. Sharma, A. B. Jha, R. S. Dubey, and M. Pessarakli, "Reactive oxygen species, oxidative damage, and antioxidative defense mechanism in plants under stressful conditions," *J. Botany*, vol. 2012, pp. 1–26, Apr. 2012.

[41] B. Meriga, B. K. Reddy, K. R. Rao, L. A. Reddy, and P. K. Kishor, "Aluminium-induced production of oxygen radicals, lipid peroxidation and DNA damage in seedlings of rice *(Oryza sativa)*," *J. Plant Physiol.*, vol. 161, no. 1, pp. 63–68, 2004.

[42] S. Mishra, A. B. Jha, and R. S. Dubey, "Arsenite treatment induces oxidative stress, upregulates antioxidant system, and causes phytochelatin synthesis in rice seedlings," *Protoplasma*, vol. 248, no. 3, pp. 565–577, 2011.

[43] C. C. Yu, "Norcantharidin triggers cell death and DNA damage through S-phase arrest and ROS-modulated apoptotic pathways in TSGH 8301 human urinary bladder carcinoma cells," *Int. J. Oncol.*, vol. 41, no. 3, pp. 1050–1060, 2012.

[44] G. Li, W. Yuan, and B. M. Fu, "A model for the blood-brain barrier permeability to water and small solutes," *J. Biomech.*, vol. 43, no. 11, pp. 2133–2140, 2010.

[45] M. Smith and Y. M. O. Gumbleton, "Primary porcine brain microvascular endothelial cells: Biochemical and functional characterisation as a model for drug transport and targeting," *J. Drug Targeting*, vol. 15, no. 4, pp. 253–268, 2007.

[46] S. Nakagawa et al., "A new blood-brain barrier model using primary rat brain endothelial cells, pericytes and astrocytes," *Neurochem. Int.*, vol. 54, nos. 3–4, pp. 253–263, 2009.

[47] M. A. McMillin, "TGFβ1 exacerbates blood-brain barrier permeability in a mouse model of hepatic encephalopathy via upregulation of MMP9 and downregulation of claudin-5," *Lab. Invest.*, vol. 95, no. 8, pp. 903–913, 2015.

[48] H. Xiong, "ABCG2 is upregulated in Alzheimer's brain with cerebral amyloid angiopathy and may act as a gatekeeper at the blood-brain barrier for A$\beta_{(1-40)}$ peptides," *J. Neurosci.*, vol. 29, no. 17, pp. 5463–5475, 2009.

[49] C. Saraiva, C. Praça, R. Ferreira, T. Santos, L. Ferreira, and L. Bernardino, "Nanoparticle-mediated brain drug delivery: Overcoming blood-brain barrier to treat neurodegenerative diseases," *J. Controlled Release*, vol. 235, pp. 34–47, Aug. 2016.

[50] H. Gao, "Progress and perspectives on targeting nanoparticles for brain drug delivery," *Acta Pharmaceutica Sinica B*, vol. 6, no. 4, pp. 268–286, 2016.

[51] T. M. Allen, "Ligand-targeted therapeutics in anticancer therapy," *Nat. Rev. Cancer*, vol. 2, no. 10, pp. 750–763, 2002.

[52] H. Gao, S. Zhang, S. Cao, Z. Yang, Z. Pang, and X. Jiang, "Angiopep-2 and activatable cell-penetrating peptide dual-functionalized nanoparticles for systemic glioma-targeting delivery," *Mol. Pharm.*, vol. 11, no. 8, pp. 2755–2763, 2014.

[53] Z. Z. Yang, "Tumor-targeting dual peptides-modified cationic liposomes for delivery of siRNA and docetaxel to gliomas," *Biomaterials*, vol. 35, no. 19, pp. 5226–5239, 2014.

[54] C. Choi et al., "Synthesis of methoxy poly (ethylene glycol)-b-poly (DL-lactide-co-glycolide) copolymer via diselenide linkage and fabrication of ebselen-incorporated nanoparticles for radio-responsive drug delivery," *J. Ind. Eng. Chem.*, vol. 47, pp. 112–120, Mar. 2017.

[55] M. E. Davis, Z. G. Chen, and D. M. Shin, "Nanoparticle therapeutics: An emerging treatment modality for cancer," *Nature Rev. Drug Discovery*, vol. 7, no. 9, pp. 771–782, 2008.